Fracture Mechanics of Thin Plates and Shells Under Combined Membrane, Bending and Twisting Loads[1]

Alan T. Zehnder
Department of Theoretical and Applied Mechanics,
Cornell University, Ithaca, NY, 14853-1503 USA
atz2@cornell.edu

Mark J. Viz
Exponent Failure Analysis Associates,
Chicago, Illinois 60606

Abstract

The fracture mechanics of plates and shells under membrane, bending, twisting and shearing loads are reviewed, starting with the crack tip fields for plane-stress, Kirchhoff and Reissner theories. The energy release rate for each of these theories is calculated and is used to determine the relation between the Kirchhoff and Reissner theories for thin plates. For thicker plates this relationship is explored using three-dimensional finite element analysis. The validity of the application of two-dimensional (plate theory) solutions to actual three-dimensional objects is analyzed and discussed. Crack tip fields in plates undergoing large deflection are analyzed using von Kármán theory. Solutions for cracked shells are discussed as well. A number of computational methods for determining stress intensity factors in plates and shells are discussed. Applications of these computational approaches to aircraft structures are reviewed. The relatively few experimental studies of fracture in plates under bending and twisting loads are reviewed.

1 Introduction

Fracture of plates and shells is of great practical as well as theoretical interest. For example, a large number of engineering structures, such as pressurized aircraft fuselages, ship hulls, storage tanks and pipelines are constructed of shells and plates. Concern over the safety of such structures has led to tremendous amounts of productive research in fracture and fatigue of structural materials. The outcomes of this research in terms of codes, design and analysis practices and better application of materials have saved countless lives and dollars.

[1]Published in Applied Mechanics Reviews, Vol. 58, pp 37-48 (2005). Updated June 12, 2008 with corrections to signs in equations 1,3,6.

Much of the research on the fracture mechanics of shells and plates has concentrated on in-plane tensile loading or on bending orthogonal to the crack. However, there are a great many practical problems involving asymmetric out-of-plane loadings, where the crack is subject to a combination of in-plane tension and out-of-plane shear. For example, in recent investigations of aging aircraft structures [1, 2, 3], fracture and fatigue under tension and out-of-plane shear loading was identified as an important, but virtually unexplored subject. In one scenario, small fatigue cracks emanating from rivet holes link up to form a macroscopic crack along a the top of a lap splice joint. As shown in Figure 1, one side of the crack will bulge out relative to the other due to the material thickness being doubled on one side and due to reinforcing elements known as stringers that are present only on one side of the crack. *Any* situation involving a crack in a pressurized shell or plate with material on one side of the crack stiffer due either to reinforcing elements, or due to curvature of the crack will result in the crack being loaded in a combination of tension and out-of-plane shear. Such cracks cannot be considered as loaded in Mode-I (in-plane tension) only.

The most general loading of a cracked plate or shell results in mixed-mode crack tip stress fields, combining in-plane tension and shear with out-of-plane bending and shear as shown in Figure 2. For elastic plates, the out-of-plane crack tip stresses can be described in terms of either three dimensional elasticity, Reissner plate theory, or Kirchhoff plate theory. Each of these descriptions, and the relation of the theories to each other will be discussed in this review. This will be followed by a discussion of computational methods and applications and finally by a discussion of experimental results for fracture and fatigue of cracked plates under bending and out-of-plane shearing loads.

2 Crack Tip Fields

Although most of the applications that motivate this work involve shells, the basic crack tip stress fields will be described in terms of plate theory. Near the crack tip, the stress distribution in shells is the same as that for plates. The shape of the shell or plate will come in only through the stress intensity factors, or constants that describe the strength of the crack tip stress singularities. Small strain, linear elastic, isotropic, homogeneous material is assumed in what follows. For now it is also assumed that there is no crack face contact. The impact of contact on the fields and on crack growth will be discussed in section 2.9.

2.1 Kirchhoff Theory

The simplest approach to the out-of-plane fracture problems shown in Figure 2 is to assume the small deflection, Kirchhoff plate theory, [4]. In the context of Kirchhoff theory, and consistent with the assumption of small deflections, the crack tip stress fields in combined in-plane and out-of-plane

loading are a superposition of the plane stress and plate theory fields [5]. In this context, each of the four loadings in Figure 2 is associated with a single independent stress intensity factor, as shown in the figure.

Using an eigenfunction approach to solve the biharmonic equations, Williams calculated the near crack tip stress and displacement fields for a crack in an infinite plate in extension [6] and in bending [7]. The stress and displacement fields with respect to the crack tip polar coordinates (r, θ) shown in Figure 3 are:

$$\left\{ \begin{array}{c} \sigma_{xx} \\ \sigma_{xy} \\ \sigma_{yy} \end{array} \right\} = \frac{K_I}{\sqrt{2\pi r}} \cos\left(\frac{\theta}{2}\right) \left\{ \begin{array}{c} 1 - \sin\left(\frac{\theta}{2}\right) \sin\left(\frac{3\theta}{2}\right) \\ \sin\left(\frac{\theta}{2}\right) \cos\left(\frac{3\theta}{2}\right) \\ 1 + \sin\left(\frac{\theta}{2}\right) \sin\left(\frac{3\theta}{2}\right) \end{array} \right\} + \frac{K_{II}}{\sqrt{2\pi r}} \left\{ \begin{array}{c} -\sin\left(\frac{\theta}{2}\right) \left[2 + \cos\left(\frac{\theta}{2}\right) \cos\left(\frac{3\theta}{2}\right)\right] \\ \cos\left(\frac{\theta}{2}\right) \left[1 - \sin\left(\frac{\theta}{2}\right) \sin\left(\frac{3\theta}{2}\right)\right] \\ \sin\left(\frac{\theta}{2}\right) \cos\left(\frac{\theta}{2}\right) \cos\left(\frac{3\theta}{2}\right) \end{array} \right\} \tag{1}$$

and

$$\left\{ \begin{array}{c} u_1 \\ u_2 \end{array} \right\} = \frac{K_I}{2\mu} \sqrt{\frac{r}{2\pi}} \left\{ \begin{array}{c} \cos\left(\frac{\theta}{2}\right) \left[2\left(\frac{1-\nu}{1+\nu}\right) + 2\sin^2\left(\frac{\theta}{2}\right)\right] \\ \sin\left(\frac{\theta}{2}\right) \left[\frac{4}{1+\nu} - 2\cos^2\left(\frac{\theta}{2}\right)\right] \end{array} \right\} + \frac{K_{II}}{2\mu} \sqrt{\frac{r}{2\pi}} \left\{ \begin{array}{c} \sin\left(\frac{\theta}{2}\right) \left[\frac{4}{1+\nu} + 2\cos^2\left(\frac{\theta}{2}\right)\right] \\ -\cos\left(\frac{\theta}{2}\right) \left[2\left(\frac{1-\nu}{1+\nu}\right) - 2\sin^2\left(\frac{\theta}{2}\right)\right] \end{array} \right\}, \tag{2}$$

where μ and ν are the shear modulus and Poisson's ratio. K_I and K_{II} are the tensile and shear stress intensity factors defined as $K_I \equiv \lim_{r\to 0} \sqrt{2\pi r}\sigma_{\theta\theta}(r, 0)$, and $K_{II} \equiv \lim_{r\to 0} \sqrt{2\pi r}\sigma_{r\theta}(r, 0)$.

The stress and deflection fields for the bending problem as calculated by Williams [7] and using the stress intensity factor definitions of Sih *et al.* [5] are [8]):

$$\left\{ \begin{array}{c} \sigma_{rr} \\ \sigma_{r\theta} \\ \sigma_{\theta\theta} \end{array} \right\} = \frac{k_1}{\sqrt{2r}} \frac{x_3}{2h} \frac{1}{3+\nu} \left\{ \begin{array}{c} (3+5\nu)\cos\left(\frac{\theta}{2}\right) - (7+\nu)\cos\left(\frac{3\theta}{2}\right) \\ -(1-\nu)\sin\left(\frac{\theta}{2}\right) + (7+\nu)\sin\left(\frac{3\theta}{2}\right) \\ (5+3\nu)\cos\left(\frac{\theta}{2}\right) + (7+\nu)\cos\left(\frac{3\theta}{2}\right) \end{array} \right\} + \frac{k_2}{\sqrt{2r}} \frac{x_3}{2h} \frac{1}{3+\nu} \left\{ \begin{array}{c} -(3+5\nu)\sin\left(\frac{\theta}{2}\right) + (5+3\nu)\sin\left(\frac{3\theta}{2}\right) \\ (-1+\nu)\cos\left(\frac{\theta}{2}\right) + (5+3\nu)\cos\left(\frac{3\theta}{2}\right) \\ -(5+3\nu)\left[\sin\left(\frac{\theta}{2}\right) + \sin\left(\frac{3\theta}{2}\right)\right] \end{array} \right\}, \tag{3}$$

$$\left\{ \begin{array}{c} \sigma_{r3} \\ \sigma_{\theta 3} \end{array} \right\} = \frac{1}{(2r)^{\frac{3}{2}}} \frac{1}{3+\nu} \frac{h}{2} \left[1 - \left(\frac{2x_3}{h}\right)^2\right] \left\{ \begin{array}{c} -k_1\cos\left(\frac{\theta}{2}\right) + k_2\sin\left(\frac{\theta}{2}\right) \\ -k_1\sin\left(\frac{\theta}{2}\right) - k_2\cos\left(\frac{\theta}{2}\right) \end{array} \right\}, \tag{4}$$

$$\sigma_{33} = 0, \tag{5}$$

and

$$w = \frac{(2r)^{\frac{3}{2}}(1-\nu^2)}{2Eh(3+\nu)}\left\{k_1\left[\frac{1}{3}\left(\frac{7+\nu}{1-\nu}\right)\cos\left(\frac{3\theta}{2}\right)-\cos\left(\frac{\theta}{2}\right)\right] + k_2\left[-\frac{1}{3}\left(\frac{5+3\nu}{1-\nu}\right)\sin\left(\frac{3\theta}{2}\right)+\sin\left(\frac{\theta}{2}\right)\right]\right\}, \quad (6)$$

where h is the plate thickness and E is the Young's modulus. The stress intensity factors k_1 and k_2 for symmetric loading (bending) and anti-symmetric loading (twisting) are defined by [5] by $k_1 \equiv \lim_{r\to 0}\ \sqrt{2r}\sigma_{\theta\theta}(r,0,h/2)$ and $k_2 \equiv \lim_{r\to 0}\ \frac{3+\nu}{1+\nu}\sqrt{2r}\sigma_{r\theta}(r,0,h/2)$.

The stress intensity factors (K_I, K_{II}, k_1, k_2) indicate the geometric movement of the crack faces with respect to each other and are summarized in Figure 2. The plane stress K_I and K_{II} refer to the familiar in-plane symmetric and anti-symmetric relative crack face displacements, respectively. The Kirchhoff bending stress intensity factors, k_1 and k_2, represent, respectively, a symmetric bending mode and an anti-symmetric twisting-transverse shearing mode. That the k_2 mode is an aggregate of both the twisting and transverse shearing modes is a direct result of the effect of the crack face Kirchhoff boundary condition, $Q_{23} - \frac{\partial M_{21}}{\partial x_1} = 0$, on the solution. Just as the transverse shear and distributed twisting moment boundary conditions cannot be separated in the Kirchhoff formulation, so too the transverse shearing and twisting modes of the crack tip displacement cannot be separated.

Because of this inherent boundary condition problem, the near tip bending stress field from Kirchhoff theory possesses some irregularities. Chief among these are two: the transverse shear stresses vary asymptotically as $r^{-\frac{3}{2}}$ instead of $r^{-\frac{1}{2}}$ as would be expected, and the ratio of $\frac{\sigma_{rr}}{\sigma_{\theta\theta}}$ for $\theta = 0$ is different for the membrane case compared to the bending case. The $r^{-\frac{3}{2}}$ transverse shear behavior is a result of the Kirchhoff formulation where the transverse shear stresses are found from third derivatives of w, the transverse displacement, whereas all other non- zero stresses are found from second derivatives of w. For $\theta = 0$, the ratio of $\frac{\sigma_{rr}}{\sigma_{\theta\theta}} = 1$ for the membrane case but $\frac{\sigma_{rr}}{\sigma_{\theta\theta}} = -\left(\frac{1-\nu}{3+\nu}\right)$ for the bending case. That the near tip stress field for membrane tension should be hydrostatic but not for bending has been viewed by most researchers to be a remnant of the Kirchhoff formulation. For these reasons, asymptotic stress fields have been found by many researchers using the Reissner [9, 10] plate formulation instead.

2.2 Reissner Theory

Knowles and Wang [11] were the first researchers to determine the Reissner asymptotic stress field for a vanishingly thin infinite plate with a center crack loaded under uniform symmetric bending. They found that for the bending problem, contrary to Williams's results, the transverse shear stress

resultants remain finite as $r \to 0$ instead of varying as $r^{-\frac{3}{2}}$. Furthermore, the ratio $\frac{\sigma_{rr}}{\sigma_{\theta\theta}} = 1$ for $\theta = 0$ just as in the generalized plane stress extension results, thereby correcting the discrepancies between the plane stress results and the bending results from the Kirchhoff theory. In an extension of this work considering finite thickness plates Wang [12] found that for the same symmetric bending problem the $r^{-\frac{1}{2}}$ stress singularity and the angular distribution of the stress fields remain the same regardless of plate thickness. However, the bending stress intensity factor was found to increase with increasing plate thickness to crack length ratio. In a very similar investigation, Hartranft and Sih [13] found for the infinite plate center crack problem under symmetric bending that for $\nu = 0.3$ and a plate thickness to crack length ratio of 0.1 the value of the bending stress intensity factor is sixty-two percent greater than the value found from Knowles and Wang's original solution which assumed a vanishingly thin plate.

Asymptotic Reissner stress field solutions also have been determined for the anti-symmetric case of a center cracked infinite plate loaded by remote twisting moments and/or transverse shear loads. Wang [14] obtained the asymptotic stress field for the twisting of an elastic plate with a center crack and again determined that all of the stresses (including the transverse shear stresses) vary as $r^{-\frac{1}{2}}$ as $r \to 0$. Furthermore, the angular distributions of the stress field were ascertained to be independent of the plate thickness and exactly the same as the familiar K_{II} sliding and K_{III} tearing modes from three-dimensional elasticity. Tamate [15] used an approach involving dislocation theory in the context of the Reissner plate formulation to determine the stress field angular variations for an arbitrarily oriented center crack in an infinite plate. Extending Wang's findings, Tamate found that the angular stress distributions for uniform bending, uniform twisting and uniform shearing are exactly the same as those from the conventional K_I opening, K_{II} sliding and K_{III} tearing modes of crack extension given that all three modes may exist for an arbitrarily oriented crack. Later, Delale and Erdogan [16] obtained the same results in every aspect as Wang for the twisting and transverse shearing of a center cracked infinite plate.

Summarizing these results from the literature, the asymptotic stress fields derived from the Reissner plate formulation provide a greater fidelity to the corresponding stress fields from three-dimensional elasticity than those obtained from the Kirchhoff plate formulation. For any type of loading— bending, twisting and/or transverse shearing—the Reissner asymptotic stress fields all vary as $r^{-\frac{1}{2}}$ as $r \to 0$, they have the same angular distributions as those from three-dimensional elasticity and these results do not change with changing plate thickness. Additionally, the effect of a finite plate thickness on the stress intensity factors is incorporated in the Reissner results and has been demonstrated to be sizable.

Again, from Hui and Zehnder [8], the Reissner asymptotic crack tip stress and displacement

fields with reference to the coordinate system of Figure 3 are:

$$\left\{ \begin{array}{c} \sigma_{rr} \\ \sigma_{r\theta} \\ \sigma_{\theta\theta} \end{array} \right\} = \frac{K_1}{\sqrt{2r}} \frac{x_3}{2h} \left\{ \begin{array}{c} 5\cos\left(\frac{\theta}{2}\right) - \cos\left(\frac{3\theta}{2}\right) \\ \sin\left(\frac{\theta}{2}\right) + \sin\left(\frac{3\theta}{2}\right) \\ 3\cos\left(\frac{\theta}{2}\right) + \cos\left(\frac{3\theta}{2}\right) \end{array} \right\}$$
$$+ \frac{K_2}{\sqrt{2r}} \frac{x_3}{2h} \left\{ \begin{array}{c} -5\sin\left(\frac{\theta}{2}\right) + 3\sin\left(\frac{3\theta}{2}\right) \\ \cos\left(\frac{\theta}{2}\right) + 3\cos\left(\frac{3\theta}{2}\right) \\ -3\sin\left(\frac{\theta}{2}\right) - 3\sin\left(\frac{3\theta}{2}\right) \end{array} \right\}, \tag{7}$$

$$\left\{ \begin{array}{c} \sigma_{r3} \\ \sigma_{\theta 3} \end{array} \right\} = \frac{K_3}{\sqrt{2r}} \left[1 - \left(\frac{2x_3}{h} \right)^2 \right] \left\{ \begin{array}{c} \sin\left(\frac{\theta}{2}\right) \\ \cos\left(\frac{\theta}{2}\right) \end{array} \right\}, \tag{8}$$

and

$$w = \frac{\sqrt{2} r^{\frac{3}{2}} (1-\nu)}{Eh} \left[K_1 \left(\frac{1}{3} \left(\frac{7+\nu}{1-\nu} \right) \cos\left(\frac{3\theta}{2}\right) - \cos\left(\frac{\theta}{2}\right) \right) \right.$$
$$\left. + K_2 \left(-\frac{1}{3} \left(\frac{5+3\nu}{1-\nu} \right) \sin\left(\frac{3\theta}{2}\right) + \sin\left(\frac{\theta}{2}\right) \right) \right]$$
$$+ \frac{8\sqrt{2r}\,(1+\nu)}{5E} \left[K_3 \sin\left(\frac{\theta}{2}\right) \right], \tag{9}$$

$$\chi = \frac{5 r^{\frac{3}{2}}}{3\sqrt{2}\,(1+\nu)} \left[K_1 \left(\sin\left(\frac{3\theta}{2}\right) + \sin\left(\frac{\theta}{2}\right) \right) \right.$$
$$\left. + K_2 \left(\frac{1}{3} \cos\left(\frac{3\theta}{2}\right) + \cos\left(\frac{\theta}{2}\right) \right) \right]$$
$$- \frac{2\sqrt{2r} h}{3} \left[K_3 \cos\left(\frac{\theta}{2}\right) \right]. \tag{10}$$

The scalar function χ is related to the transverse shear resultants by

$$Q_{13} = \frac{\partial \chi}{\partial x_2}, \quad Q_{23} = -\frac{\partial \chi}{\partial x_1} \tag{11}$$

and further is used in the equations for the in-plane displacements

$$u_\alpha = -x_3 \frac{\partial w\,(x_1, x_2)}{\partial x_\alpha} + \frac{12\,(1+\nu)}{5Eh} x_3 Q_{\alpha 3}\,(x_1, x_2) \tag{12}$$

where $\alpha = 1, 2$. The stress intensity factors (K_1, K_2, K_3) are referred to as the Reissner stress intensity factors, and are defined by $K_1 \equiv lim_{r\to 0}\sqrt{2r}\sigma_{\theta\theta}(r, 0, h/2)$, $K_2 \equiv lim_{r\to 0}\sqrt{2r}\sigma_{r\theta}(r, 0, h/2)$, and $K_3 \equiv lim_{r\to 0}\sqrt{2r}\sigma_{\theta 3}(r, 0, 0)$. For both the Kirchhoff and Reissner theories several different notations and definitions of the stress intensity factors can be found in the literature.

Note that the w field of the Reissner theory contains both the $r^{3/2}$ Kirchhoff w field and an $r^{1/2}$ field. Thus very near the crack tip the displacement field varies as $r^{1/2}$. Away from the crack tip the $r^{3/2}$ term of the Kirchhoff theory dominates.

At this point one might pose the question of which theory and hence set of stress intensity factors should be used to describe crack tip stresses and to correlate fracture initiation and growth?

The Kirchhoff theory is simpler, but due to the kinematic assumption that lines perpendicular to the plate surface remain perpendicular (analogous to plane sections remain plane in beam theory), stress free boundary conditions on the crack cannot be exactly satisfied. By allowing lines perpendicular to the plate to rotate and deform, the Reissner theory introduces additional kinematic flexibility that allows stress free boundary conditions to be satisfied exactly. Thus it would appear that the Reissner theory is a better choice for describing the crack tip stress fields. However, it is known that solutions from the Reissner and Kirchhoff theories differ near free edges only in a boundary layer of extent on the order of the plate thickness. Within this boundary layer, for ductile materials, plastic deformation occurs, thus neither elastic plate theory is valid. Furthermore, as discussed in the next section, in the limit as the plate thickness goes to zero the energy release rate is the same from either theory. Thus Hui and Zehnder [8] argued that consistent with the small scale yielding approach to fracture, the Kirchhoff theory is a valid choice for correlating the fracture behavior in thin plates; it correctly describes the stress field in a region outside the crack tip plastic zone, provides the correct energy release rate, and is easily used for engineering analyses. For thick plates the Reissner theory, or even fully three-dimensional elasticity theory must be used.

2.3 Energy Release Rate

Given the assumption of small scale yielding, the energy release rate, G, is equal to the energy of newly created crack surface per unit area which, given the further assumptions of linear elastic behavior, is related to the work done by the tractions acting over the area of crack extension, see Irwin [17] and Rice [18]. For a plate of thickness, h, with the further restriction that the increment of crack growth must be self-similar, i.e., it must remain in the x_1, x_3 plane with the crack front straight through the thickness and normal to the midplane, the energy release rate may be expressed as [19]

$$G = \lim_{\Delta L \to 0} \frac{1}{2h\Delta L} \int_0^{\Delta L} \int_{-\frac{h}{2}}^{+\frac{h}{2}} \sigma_{2i}\left(x_1, \theta = 0, x_3\right) \Delta u_i \left(\Delta L - x_1, \theta = \pm\pi\right) dx_3 dx_1, \tag{13}$$

where $i = 1, 2, 3$ and indicates summation in the usual sense. The Δu_i term represents the difference in corresponding displacement components for crack growth of ΔL, i.e.,

$$\Delta u_i = u_i \left(\Delta L - x_1, \theta = +\pi\right) - u_i \left(\Delta L - x_1, \theta = -\pi\right). \tag{14}$$

For a geometrically nonlinear global behavior although explicit statements for σ_{2i} and u_i are generally unavailable, Lemaitre et al. [20] have shown that eq. 13 is still valid as long as the material behavior is elastic.

2.3.1 G for Superposition of Plane Stress and Kirchhoff Theory

Substituting the plane stress fields and the Kirchhoff plate theory fields into eq. 13 the total energy release rate is [21, 8]

$$G = \frac{1}{E}\left(K_I^2 + K_{II}^2\right) + \frac{\pi}{3E}\left(\frac{1+\nu}{3+\nu}\right)\left(k_1^2 + k_2^2\right). \tag{15}$$

Equation 15 relates the total energy release rate for self-similar crack growth in a thin plate to the K_I and K_{II} modes, representing the membrane contributions to G, and to the k_1 and k_2 modes, representing the bending and twisting-transverse shearing contributions to G.

2.3.2 G for Superposition of Plane Stress and Reissner Theory

For the Reissner theory fields, a similar result is obtained [22, 8]

$$G = \frac{1}{E}\left(K_I^2 + K_{II}^2\right) + \frac{\pi}{3E}[K_1^2 + K_2^2 + K_3^2\frac{8(1+\nu)}{5}]. \tag{16}$$

2.4 Relation Between Kirchhoff and Reissner Theory Stress Intensity Factors for Thin Plates

Simmonds and Duva [23] showed that as $h/a \to 0$, where a is the crack length and h is the plate thickness, the energy release rates from the Reissner theory and the Kirchoff theory are the same. Using this result we can obtain a universal relation between the Reissner and Kirchhoff theory stress intensity factors for thin plates.

Consider first symmetric bending loading. In this case the only non-zero stress intensity factors are k_1 for the Kirchhoff theory and K_1 for the Reissner theory. Equating the energy release rates one obtains

$$K_1/k_1 = [(1+\nu)/(3+\nu)]^{1/2}. \tag{17}$$

The validity of eqn 17 is verified by the extremely precise numerical solutions for K_1 as a function of h/a by Joseph and Erdogan [24]. Their results agree with the theoretical results to within five significant figures.

For anti-symmetric bending the non-zero stress intensity factors are k_2 for Kirchhoff theory and $K_2,\ K_3$ for the Reissner theory. Again, equating energy release rates,

$$k_2^2\frac{1+\nu}{3+\nu} = K_2^2 + K_3^2\frac{8(1+\nu)}{5}\ . \tag{18}$$

The above proves that K_2 and K_3 cannot be independent for thin plates. In practice this means that there is no loading that can produce only K_2 or only K_3 stress intensity factors.

2.5 Stress Intensity Factor Solutions

Kirchhoff theory stress intensity factors solutions for an array of geometries and loadings of infinite and finite plates are tabulated in the handbook edited by Murakami [25]. However, some of these solutions are incorrect, including the results for a finite crack in an infinite plate. Consider a crack of length $2a$ oriented at angle β to the axis of loading, as shown in Figure 4. The far field loading is either uniform transverse shear, Figure 4a, or uniform bending, Figure 4b. Using conformal mapping Zehnder and Hui [26] show that for transverse shear loading of magnitude Q_0,

$$\begin{aligned} k_1 &= \frac{3Q_0 a^{3/2} \nu \cos\beta}{h^2}, \\ k_2 &= \frac{3Q_0 a^{3/2} \sin\beta}{h^2}, \end{aligned} \tag{19}$$

and for bending of magnitude M_0,

$$\begin{aligned} k_1 &= \frac{6M_0 \sin^2\beta\sqrt{a}}{h^2}, \\ k_2 &= 0. \end{aligned} \tag{20}$$

The above equations represent a correction to the results published by Sih *et al.* [5].

Note that for many problems involving cracked plates of finite size, the stress intensity factors k_1 and k_2 are generally coupled, that is, both stress intensity factors are present. For example, using conformal mapping, Hasebe *et al.* [27] calculated the normalized k_1 and k_2 for a cracked, stepped strip under bending. The inherent asymmetry of the geometry results in both k_1 and k_2 being nonzero. Similar results are obtained for torsional loading of the strip. This is also true of real world applications in which the crack tip will generally be subjected to mixed-mode loading, i.e. more than one of the stress intensity factors is non-zero.

Solutions for Reissner stress intensity factors are available for various problems involving infinite plates [12, 14, 15, 24, 28], and plates of finite dimensions [29, 30]. The stress intensity factors are calculated through the solution of integral equations and by using boundary collocation. These and other results are tabulated in handbooks [25, 31]. Unlike problems for Kirchhoff theory, the stress intensity factors for Reissner theory plates depend strongly on the thickness of the plate relative to the crack length or other characteristic in-plane dimension.

2.6 Comparison of Plate Theory Solutions to Three Dimensional Elasticity Theory Results

Plate theories are an approximation of the three dimensional theory of elasticity. They do a good job of estimating stresses and deformations globally, but not necessarily of capturing details of the

stresses near edges and with complex boundary conditions. Thus one might pose the question of given that any physical fracture problem is three dimensional, to what degree of fidelity do either of the plate theories discussed above describe the crack tip stress fields?

Alwar and Ramachandran [32] used three dimensional finite elements to compute the through thickness variations of $K_I,\ K_{II}$ and K_{III}. These results are compared to the Reissner theory stress intensity factors, $K_1,\ K_2,$ and K_3, and show that the Reissner theory underestimates the crack tip stresses by 5-10%, depending on the plate thickness. Barsoum [33] used a singular 20 node degenerate solid element to calculate stress intensity factors in a plate under pure bending. Rhee and Atluri [34] used a hybrid stress finite element procedure to calculate stress intensity factors based on Reissner theory.

Zucchini *et al.* [35] used three dimensional finite element analysis to study the near tip fields in plates under bending, shear and twisting loads. As shown in Figure 5 for symmetric bending the Reissner theory is accurate near the crack tip ($r/h < 0.1$). However, it diverges from the actual stress field away from the crack $r/h > 1$, where the Kirchhoff theory predicts the stresses very accurately. As discussed in section 2.1, note that the Kirchhoff theory predicts the wrong sign of the normal stress σ_{11} parallel to the crack. For a plate with $a/h = 100$, both plate theories underestimate the energy release rate by a few percent compared to the actual 3D elasticity theory results. Both plate theories predict a linear through-the-thickness stress variation. This variation is confirmed, even very near the crack tip ($r/h < .002$). Mullinix and Smith's [36] frozen stress photoelasticity studies also confirm the validity of the linear stress distribution near the crack tip.

Under shear and twisting loading, the stress fields become more complex and near the crack tip are not as well described by either plate theory. Shear stresses computed by FEA ahead of a crack in a plate under shear loading are shown in Figure 6 and compared to the Kirchhoff theory results. For such thin plates Reissner theory stress intensity factors cannot be found in the literature, and thus are not plotted in the figure. Close to the crack tip the Kirchhoff theory predicts the wrong sign for the out-of-plane shear stress, however for $r/h > 1$, the Kirchhoff theory is accurate. For shear loading, both the Kirchhoff and Reissner theories predict that the out-of-plane shear stresses, $\sigma_{13},\ \sigma_{23}$ should vary parabolically through the thickness of the plate while the in-plane shear stresses, σ_{12} should vary linearly through the thickness. While the linear variation of σ_{12} near the crack tip was confirmed by the 3D FEA study, the results showed that the parabolic distribution is not accurate near the crack tip for σ_{13}. Figure 7 plots the through-the-thickness variation of $\sigma_{13}(x_3)/\sigma_{13}(x_3 = 0.065h/2)$ for a cracked plate of thickness h subjected to uniform far field shear. Very near the crack tip, $r/h = .0013$, the shear stress is nearly uniform. Not until $r/h = 0.303$ does σ_{13} become parabolic as predicted by plate theory. For twisting of a thin plate the through-

the-thickness stress results are even more complex than the shear case. Very near the crack tip σ_{12} is not linear as predicted by both plate theories; instead it is somewhat reduced as the free surface $x_3 = \pm h/2$ is approached. The out-of-plane shear stress σ_{13} parabolic only for $r/h > 0.25$.

Equation 18 suggests that there is a universal relation between k_2 and a combination of K_2 and K_3. Interpreting the through the thickness variations of stresses in the shear problem in the context of Reissner theory, K_3/k_2 and K_2/k_2 where computed and plotted against each other. Fitting a straight line to this data a linear relationship

$$k_2 = a_2 K_2 + a_3 K_3 \ , \tag{21}$$

where $a_2 = 1.42$, and a_3=1.87 was found. Note that as h/a gets smaller (thinner plate) $K_3/k_2 \to 0$, consistent with results of Tamate [15] that show K_3 going to zero for thin plates.

2.7 Crack Tip Fields in von Kármán (Large Deflection) Theory

The assumption of small deflections used in the above descriptions enables the membrane stresses due to in-plane loading to be decoupled from the stresses due to bending, twisting and shearing loading. Although this simplifies the analysis, this assumption limits the application of these theories to structures in which the deflections are small. Although this has not stopped anyone from applying plate theories of fracture to large deflection problems, it leads to the question: Do the Kirchhoff theory fields still describe the crack tip stresses when large deflections occur, and if so, how do we determine the stress intensity factors? We can ask the same question about stresses in shells versus plates.

The first question was answered by Hui *et al.* [37] by performing an asymptotic analysis in the context of the large deflection plate theory developed by von Kármán [38]. The asymptotic analysis shows that the Kirchhoff theory fields, eqns. (3-6), still apply for the case of a von Kármán plate. This, however, does not imply that the stress intensity factors can be determined by the linear theory. They can only be determined by solving the full set of nonlinear, coupled equations.

For complex geometries these equations must be solved numerically using geometrically non-linear finite element analysis, interpreting the crack tip stresses in the context of the linear theory. This is an example of the global-local approach found in many structural analysis problems, for example the work of Johnson [39] on failure of lap shear joints. For simple geometries closed form solutions can be obtained. Hui *et al.* [37] found solutions for a clamped, infinite strip containing a semi-infinite crack and for a small crack in a circular plate. Two loadings of the infinite strip are considered, pressure and shear. The results show how in this case the membrane and Kirchhoff theory stress intensity factors are coupled and how they vary with geometry and loading. For

example, for shear loading of the strip, at small loads $K_I = 0$, and $k_2 \sim w$, where w is the shearing displacement applied on one edge of the strip. As the loading progresses, membrane stresses build up and $k_2 \to 0$, while $K_I \sim w^2$.

2.8 Cracks in Thin Shells

Early experimental results from Frisch [40] on flat and curved aluminum panels with stiffeners running parallel to a crack have shown that panels with a sixty-nine inch radius of curvature fail at roughly a forty percent lower uniaxial tensile stress than corresponding flat panels both having approximately equal initial crack length to panel width ratios. Although these had been stiffened panels, it is evident from these results that curvature strongly influences residual strength. In developing a fracture criterion for pressure vessels Folias [41] also has discovered that "shells present a reduced resistance to fracture initiation that is basically of geometric origin."

For unstiffened pressure vessels Folias calculated the near tip stress fields for a crack in a pressurized spherical shell [42], for an axial crack in a pressurized cylindrical shell [43] and for a circumferential crack in a pressurized cylindrical shell [44]. Having been motivated by the fact that it is generally easier to conduct experiments on flat plates rather than curved shells Folias's objective had been to determine if curved shell behavior could be found from corresponding flat plate experimentation.

In particular, we reference Folias's results from his analysis of an axial crack in a pressurized cylindrical shell [43]. For this problem, using linear shallow thin shell theory, Folias has found that the stresses σ_{11}, σ_{12} and σ_{22} for both bending and extension vary as $r^{-\frac{1}{2}}$ as $r \to 0$ along the crack line, that these stresses have the same angular distribution as those for a flat plate and that the stress intensity factors are functions of the radius of curvature. Furthermore, as the radius of curvature approaches infinity, the flat plate solution is recovered. The bending and extensional crack tip stresses are found to be functions of both the membrane and bending boundary conditions; this coupling results from the incorporation of curvature terms in the governing equations and not from an explicit treatment of geometrically nonlinear behavior. For example, an axial crack loaded by both internal pressure and extensional in-plane load experiences a crack tip stress field that has both extensional and bending components. In other words, because of initial curvature, an applied extensional load generates both bending and extensional stresses. An applied bending load does the same. This bending- extension interaction disappears when the radius of curvature approaches infinity and the shell wall thickness approaches zero. Finally, Folias has given a general expression

relating the near tip stress fields in cylindrical shells to those in flat plates by

$$\frac{\sigma_{shell}}{\sigma_{plate}} \approx 1 + \left(a + b \ln \frac{c}{\sqrt{Rh}} \right) \frac{c^2}{Rh} + \bigcirc \left(\frac{1}{R^2} \right) \tag{22}$$

where c is the half crack length, R is the radius of curvature, h is the wall thickness and a and b are undetermined constants. Since the expression in parentheses is stated to be positive, the conclusion is that the overall effect of initial curvature is to *increase* the stress in the region near the crack tip.

In an extension of previous work Folias [45] generalized his results by calculating the asymptotic stress fields for cracked conical and toroidal shells as well as for arbitrarily oriented cracks in cylindrical shells. In all cases he has found that the increase in stress near the crack tip given by the form of Equation 22 occurs as a result of the effect of the initial curvature. More exact solutions considering a broader range of parameters than those presented by Folias for the axial crack problem in a pressurized cylindrical shell have been obtained by Copley and Sanders [46] for an unstiffened cylindrical shell and by Duncan and Sanders [47] for a cylindrical shell with a circumferential stiffener proximate to the axial crack. Yashhi and Erdogan [48] calculated the stress intensity factors for a cylindrical shell with an inclined crack. Solutions for circumferential cracks in cylindrical shells under internal pressure and external loads are given in [49, 50, 51, 52]. Stress intensity factors for an arbitrarily oriented crack in a shallow shell were computed by Simmonds *et al.* [53]. These and other solutions are tabulated in Murakami [25]. Additional review of shell fracture problems may be found in ref. [54].

Although the solutions found by Folias for the crack problems just discussed provide a good deal of information about the nature of the asymptotic stress fields and the form of the bending-extension coupling they are valid only for very small values of the shell parameter, λ. This shell parameter is commonly defined as

$$\lambda = \left[12 \left(1 - \nu^2 \right) \right]^{\frac{1}{4}} \frac{c}{\sqrt{Rh}}, \tag{23}$$

where c is the half crack length, R is the radius of curvature and h is the shell wall thickness. For values of λ greater than unity solutions to the cracked shell problems of Folias have been computed numerically (without geometric nonlinearity) by Erdogan and Kibler [55] and Erdogan and Ratwani [56]. Their results assume that only the crack faces are loaded, either extensionally in-plane or by bending moments; in this way, "the singular solution of the cracked shell problem may be reduced to a perturbation problem in which self-equilibrating forces and moments acting on the crack surfaces are the only external loads" [55].

Recent work on fracture of cracked shells has concentrated on computational methods where it

is possible to account for the important geometric nonlinearities that occur in practical structures. This will be discussed in section 3.

2.9 Effect of Crack Face Contact During Bending

In bending of a plate with a through crack, the crack faces will come into contact unless sufficient membrane tension, K_I is applied. When this occurs, it is clear that contact of the crack faces will introduce additional loads along the crack line and will change the crack tip stress and displacement fields. Numerous analytical, computational and experimental efforts have been made to address this issue.

Smith and Smith [57] first studied this problem experimentally using frozen stress photoelasticity. They concluded that crack face contact during bending increased the crack tip stress over the no contact case. Jones and Swedlow [58] performed an elastic-plastic finite element analysis of crack face contact during bending. They assumed Kirchhoff kinematics and power law hardening. Contact was modelled by requiring that the displacement perpendicular to the crack, on the compressive side of the plate, is zero. This is an example of a line contact model. The model results in a constraint equation, $u_2(x_1, x_2) - x_3[\partial w(x_1, x_2)/\partial x_2] = 0$, that was introduced to the computational procedure through the use of Lagrange multiplier concepts. They find that closure increases the tension side stress intensity factor by about 20%. Young and Sun [59] performed a line contact analysis for Kirchhoff theory. Heming [60] performed an elastic analysis of contact during bending, using finite elements with Reissner theory kinematics, and assuming a line contact model as in the Jones and Swedlow analysis. Heming finds that due to the moment on the crack face induced by closure, the rotation of the crack flank about the x_1 axis and the opening displacement are reduced. In contrast with Jones and Swedlow, Heming's analysis shows that closure reduces the crack tip stresses on the tensile side. Heming argues that this difference is due to the boundary condition inaccuracies inherent in Kirchhoff kinematics. Alwar and Ramachandran [61] performed a three dimensional finite element analysis of this problem. By iteration they were able to accurately determine the actual area of contact. As with Heming's line contact model, they find that closure reduces the crack tip stress intensity, although by an amount that is smaller than the line contact model predicts. Murthy *et al.* [62] consider line contact for Reissner theory kinematics. Their method is based on a combination of finite element and analytical solutions. Murthy *et al.* predict a reduction in stress intensity factor due to contact that is similar to the 3D results of Alwar and Ramachandran.

Delale and Erdogan [63] and Joseph and Erdogan [24] consider a line spring model of contact for both Kirchhoff and Reissner theories. The problem is formulated and solved in terms of singular

integral equations. They show that the stress intensity factor is reduced due to crack contact by an amount that agrees well with the 3-D FEM results of Alwar and Ramachandran. Young and Sun [21] used integral equations to solve the line contact model in the context of Reissner theory. Consistent with the above results they find that contact reduces crack tip stresses by a larger amount than predicted by 3D analysis. Slepyan *et al.* [64] and Dempsey *et al.* [65] solve for area contact using Reissner theory. They investigate the effects of plate thickness and of remote loading on the size and shape of the contact region and on the crack tip stresses. In attempting to correlate their results with Smith and Smith's data from thirty years ago, they point out the need for fundamental experimental research in the fracture of plates under bending and membrane loading.

3 Computational Methods and Applications for Plates and Shells

To determine the stress intensity factors and hence to predict fracture initiation and growth in structures a general purpose computational approach is needed that can deal with mixed mode loadings and with geometrically nonlinear shell structures. Such an approach must be efficient, accurate and adaptable to a large number of structural and material systems.

3.1 Computing Stress Intensity Factors and Energy Release Rate

Viz *et al.* [19] investigated the use of standard, 4 noded shell elements in a general purpose finite element code to compute Kirchhoff theory stress intensity factors for plates. They applied the methods of virtual crack extension (VCE) [66], nodal release, (NR) [67] and modified crack closure, (MCCI) [68], to compute stress intensity factors for a finite crack in an infinite sheet under membrane, bending and out-of-plane shearing loads. Using any of these methods, stress intensity factors for the membrane loadings and for shear loadings could be computed to within 1% accuracy using square elements of length $a/64$, where a is the half crack length. For shear loading the accuracy was only 3.6%. The MCCI approach was extended to large deflections and to 8 noded elements by Viz [69] and by Hui *et al.* [37]. Viz's approach has the great advantage that it can be used with any commercial finite element code that supports geometrically nonlinear plate and shell computations. No special elements are required, and only a moderately fine mesh is required for all problems except the out-of-plane shear case.

For small deflections of a plate, and Frangi and Guiggiani [70, 71] have developed boundary element methods that provide very high accuracy using only a small number of boundary elements. However, this method cannot be extended to large deflections, and is thus of limited practical application to structures.

Su and Sun [72] used the fractal finite element method, or FFEM, to accurately compute stress intensity factors in thin plates under bending, twisting and shear loads. In this approach, the crack tip singularity is built into the solution of the problem through a special, fractal, crack tip element. This method should be extensible to large deformation and to thick plate problems.

Other approaches to computing stress intensity factors in symmetric bending problems include the work of Wilson and Thompson [73] who computed stress intensity factors for symmetric bending using displacement correlation, Chen and Chen [74], who used singular elements, and Chen *et al.* [75] who used the finite element alternating method. Ahmad and Loo [76], and Chen and Shen[77] considered the mixed mode bending problem and computed k_1 and k_2. For antisymmetric bending, or constant remote twisting moment, their results agreed with the k_2 result of Sih *et al.* [5], despite the errors in this solution found and corrected by Zehnder and Hui [26], and given as eqn. (20) in this paper. The results of Su and Sun are in agreement with Zehnder and Hui's correct results. Chen and Shen replaced the constant twisting moment on the crack faces with a shear distribution designed to give the value of k_2 from Sih's paper. Thus, since Sih's result is actually part of Chen and Shen's FEM formulation, they reproduce this result even though it is incorrect. It is unclear why Ahmad and Loo's results disagree with Zehnder and Hui's theoretical results. It appears that the incorrect theory is built into their computational framework.

Dolbow *et al.* [78] developed an efficient approach and have implemented it in the context of Reissner (thick plate) theory. There are two key ideas to Dolbow's work. Rather than use pointwise methods such as NR and MCCI, the interaction integral, Yau *et al.* [79], a J-integral type approach, was developed to compute components of energy release rate over an area surrounding the crack tip. This allows the extraction of mixed-mode stress intensity factors with high accuracy relative to using MCCI or other methods for the the same element size. The second idea is to use enriched elements in which the crack tip displacement and rotation fields are embedded into the shape functions of the elements in the region of the crack. It is not necessary in this approach for the mesh to model the crack discontinuity; "the jump in the rotations and transverse displacement is created entirely with enrichment." The finite element results are compared to results for a finite crack in an infinite plate under bending. The FEM simulations are within a few percent accuracy for all cases, requiring modest mesh density. This method can be extended to large deflections and should also be extendable to thin shells and plates.

Dirgantara and Aliabadi [80, 81] developed a boundary element formulation for computing stress intensity factors in shells in the context of Reissner plate theory. Stress intensity factors are computed based on the boundary element results using the crack surface displacement extrapolation method and by calculating energy release rates using the known relationships between G and the

stress intensity factors. Highly accurate results are obtained with these methods. This method was applied [82] to analyze stiffened panels [83] and applied to the prediction of fatigue crack growth in a pressurized, cylindrical shell.

3.2 Computational Mechanics Applications

There have been a number of applications of computational methods to problems in aircraft structural integrity. Riks and denRijer [84], Riks [85], and Chen and Schijve [86] have all studied the so-called "crack bulging" problem. The deformation of a crack in a pressurized cylinder is resisted by both membrane and bending stiffness. For the case of the cylinder, the crack faces consequently deform both in the tangent plane of the crack line and normal to it. This normal component is referred to by Riks and many others as "crack bulging." As the pressure in the cylinder increases so does the bulging deformation but in a nonlinear fashion with pressure. A doubling of the pressure does not double the bulging deformation. Instead, this bulging is resisted to greater degrees by the in-plane membrane stresses that become large at higher pressures; this situation is analogous to the large deflection of a flat plate. In work on stiffened, cracked, pressurized cylinders Riks determined, in agreement with earlier results of Folias [43], that cracks in cylinders have higher stress intensities than corresponding cracks in similar flat plates and that the linear shell solutions of Folias "considerably overestimate" the actual stress intensities computed from a geometrically nonlinear analysis.

Chen *et al.* [87, 88] have combined geometrically nonlinear, elastic-plastic shell analysis with adaptive remeshing to study crack tearing in stiffened shell structures. Computations of stress intensity factors versus crack extension in a fuselage show that in the context of a superposition of Kirchhoff and Reissner theories, the crack tip stresses can be characterized by a combination of all four stress intensity factors, $K_I,\ K_{II},\ k_1,$ and k_2. For a crack that starts along a fuselage lap joint, as the crack curves, or flaps, the stresses are dominated by the K_I and k_2 stress intensity factors. By taking into account T-stress (stress parallel to the crack line) and fracture toughness orthotropy (due to processing of the aluminum sheet) predicted crack paths agreed reasonably well with measured paths. Residual strengths are computed based on a critical crack tip opening angles (CTOA) approach and with consideration of multi-site damage (MSD), simulated by seeding the problem with cracks emanating from fastener holes.

Huang, Li and Russell [54] review the theory of fracture of plates and shells and apply the theory to study the problem of fracture of a fuselage under various loadings, including internal pressure, bending and shearing [89]. Using the virtual crack extension method in conjunction with shear deformable shell elements the energy release rates for various loadings of a longitudinal

crack in a stiffened fuselage are computed. The effects of geometrical nonlinearity are explored by comparing linear and nonlinear solutions. For cracks loaded by internal pressure, the linear theory underestimates the energy release rate.

4 Experimental Observations of Fracture in Plates and Shells

One of the first experimental studies of fracture in bent plates was performed by Erdogan *et al.* [90] who tested cracked PMMA sheets in pure bending and found that k_1 works well to correlate fracture toughness data. Wynn and Smith [91] measured the failure load of PMMA plates in tension and bending and attempted to correlate the data with failure theories based on energy release rate and maximum tensile stress. Smith and Smith [57] used frozen stress photoelasticity to investigate the stress fields in bending. Saint-John and Street [92] have used a double-edge notched specimen to study the fracture toughness of boron-aluminum compressor blades loaded in tension and torsion; their results exhibit a significant loading path dependence on fracture loads. Lemaitre *et al.* [20] performed flat panel fatigue tests under cyclic tension and pressure and observed that the rate of crack growth is accelerated relative to tension only.

Ewing and Williams [93] performed fracture experiments on pressurized, spherical caps made of polymethylmethacrylate (PMMA). Their test samples had a through crack at the top of the shell. The cracks were sealed against leakage by using a thin metal strip and plasticine. The shells were pressurized until the point of unstable fracture. By performing a number of experiments for different crack lengths and shell radii, Ewing and Williams were able to show that the fracture data are well correlated by Folias's theory [42].

Bastun [94] studied the fracture of pre-cracked cylindrical shells of titanium and steel loaded with static and cyclic internal pressure and external tension or compression. Increasing the axial tension resulted in an increase in the pressure needed to cause unstable crack growth and decreased the rate of fatigue crack growth, demonstrating the nonlinear effect of axial tension in suppressing crack tip hoop stresses. The opposite effect was demonstrated for axial compression.

Viz, Zehnder and Bamford [95, 69, 96] performed an extensive set of experiments on fatigue crack growth in thin plates under tension and out-of-plane shear loads, or K_I and k_2 in terms of stress intensity factors. The test specimen was a double edge notched sheet of 0.09 in. thick 2024-T3 Al. The samples were loaded in in-phase tension and torsion to provide various mixes of K_I and k_2 stress intensity factors, mimicking the stresses at the tip of a lap joint crack in a pressurized fuselage. Results of the experiments are shown in Figures 8-10, which plot the crack growth rate per cycle, da/dN versus ΔK_I, where $\Delta K_I = K_I^{max} - K_I^{min}$ during a cycle. The data from many tests are given in three plots separated by the ratio of $\Delta k_2/\Delta K_I$. In Figure 8, where

$\Delta k_2/\Delta K_I < 0.4$ the crack growth rate generally starts out close to the pure Mode-I benchmark, but then drops and fluctuates as the crack extends past a distance of approximately 0.7 *in.* In Figure 9, where $0.4 < \Delta k_2/\Delta K_I < 0.7$ the initial rate of growth is somewhat higher than the pure Mode-I case. Again, as the crack extends past approximately 0.7 *in.* the rate drops and fluctuates. Figure 10 shows the results for $0.7 < \Delta k_2/\Delta K_I < 1.0$ Here da/dN is initially much higher than the pure Mode-I case, but drops dramatically as the cracks grow.

The general observation is that in the presence of out-of-plane shear loading, k_2, the rate of crack growth drops as the crack grows. This was observed to be associated with the crack faces contacting each other during the fatigue tests. Examination in a scanning electron microscope revealed regions of abrasion and wear on the crack faces. As shown in Figure 11, crack face contact is due both to fracture surface roughness and due to slant crack growth that occurs as a result of the unique stress fields caused by k_2 loading.

To quantify the reduction in growth rate due to contact of the crack faces a series of experiments were performed in which the crack wake was artificially removed. This allow the intrinsic crack growth rate, i.e. the growth rate under mixed-mode loading in the absence of contact, to be determined and to be contrasted with the growth rate in the presence of contact. The results of these experiments are summarized in Figure 12. The dashed line shows the intrinsic crack growth rate. The straight solid line is the benchmark, or pure tension (K_I) crack growth rate. The points show how crack growth rate decreases in each of several tests as the crack grows. The results show that in the absence of crack face contact, the presence of k_2 loading increases the crack growth rate substantially over the pure tension loading case. As the crack grows and the region of contact behind the crack develops, the growth rates drop to well below the pure mode I rates.

Similar results are observed in the context of mixed mode fatigue of cracked shafts under tension (K_I) and torsional (K_{III}) loads, Tschegg *et al.* [97, 98]. The main conclusion from these studies is that nominal ΔK_{III} does not correlate torsional fatigue crack growth rate data. Using a relatively simple frictional model Gross [99] was able to simulate the effect of frictional shielding of the crack tip and was able to correlated mixed-mode crack growth rate data.

As sketched in Figure 11 cracks generally grow on a slant, or in many cases in a V-shape. It is observed that when cracks grow in a V-shape they always curve (propagate with a y component in Figure 11). This is presumably caused by non-zero values of K_{II} at the tip of the V-shaped crack, although no detailed analysis of this problem has been performed.

5 Outstanding Research Issues

The three dimensional elasticity stress fields near the tip of a crack under bending, extension and twisting loads are well known from detailed finite element computations. However, comparable studies have yet to be performed for the more realistic and complex problem of elastic-plastic fracture. Using a small scale yielding analysis in which the elastic fields are imposed as far field boundary conditions in a manner analogous to Narasimhan and Rosakis [100] the size and shape of the crack tip plastic zone should be determined. Relaxing the small scale yielding constraint, the extent of validity of the small scale yielding model should be determined. As mentioned, in general cracks go not grow with their surface perpendicular to the plane of the plate. Thus the case of slanted and V-shaped cracks must be studied to examine the application of small scale yielding to this realistic situation, i.e. to answer the question of whether stress intensity factors still uniquely characterize the crack tip fields, and if not, what parameters are needed to describe the fields and to correlate fracture initiation and growth data.

It is unrealistic to expect that the complex problem of fatigue crack growth in an elastic-plastic material can be correlated with stress intensity factors if for the far simpler problem of fracture initiation from a sharp crack in a brittle material cannot be correlated. Extensive searches of the literature reveal no studies of the basic problem of fracture initiation under K_I and k_2 loading. Such a set of experiments should be performed; the solutions of Hui and Zehnder [37] can serve as a starting point for specimen design and calibration.

As the results of Figures 8, 9, 10 and 12 demonstrate, contact and the resulting friction behind the crack tip greatly reduce fatigue crack growth rate. Although this is well understood qualitatively, there exist no demonstrated modeling approaches that would allow us to correlate fatigue crack growth rate data with (K_I, k_2). A method for measuring and modelling the evolution of crack face contact and friction in the wake of the crack should be developed. Once such a model is known, it should be implemented in a computational code to predict the actual crack tip stress intensity factors and hence to correlate fatigue crack growth under (K_I, k_2) loadings.

6 Acknowledgements

The first author would like to thank his colleagues Profs. Hui and Ingraffea at Cornell for their contributions and discussions and to thanks Drs. Harris and Newman at NASA Langley for supporting and providing context to this research.

References

[1] Potyondy D (1993), *A Software Framework for Simulating Curvilinear Crack Growth in Pressurized Thin Shells*, Ph.D. thesis, Cornell University, School of Civil and Environmental Engineering Report No. 93–5.

[2] Potyondy D, Wawrzynek P, and Ingraffea A (1994), Discrete crack growth analysis methodology for through cracks in pressurized fuselage structures, in Harris C (ed.) *FAA-NASA International Symposium on Advanced Structural Integrity Methods for Airframe Durability and Damage Tolerance*, vol. 2, 581–601, NASA CP3274.

[3] Harris CE, Newman JC, Piascik RS, and Starnes JH (1997), Analytical methodology for predicting the onset of widespread fatigue damage in fuselage structure, *FAA-NASA Symposium on the Continued Airworthiness of Aircraft Structures* **DOT/FAA/AR-97/2**, 63–88.

[4] Kirchhoff G (1850), Über das gleichgewicht und die bewegung einer elastischen scheibe, *J für Reine und angewandte Mathematik* **40**, 51–88.

[5] Sih G, Paris P, and Erdogan F (1962), Crack-tip stress-intensity factors for plane extension and plate bending problems, *Journal of Applied Mechanics* **29**, 306–312.

[6] Williams M (1957), On the stress distribution at the base of a stationary crack, *Journal of Applied Mechanics* **24**, 109–114.

[7] Williams M (1961), The bending stress distribution at the base of a stationary crack, *Journal of Applied Mechanics* **28**, 78–82.

[8] Hui CY and Zehnder A (1993), A theory for the fracture of thin plates subjected to bending and twisting moments, *International Journal of Fracture* **61**, 211–229.

[9] Reissner E (1945), The effect of transverse shear deformation on the bending of elastic plates, *Journal of Applied Mechanics Trans ASME* **67**, A69–A77.

[10] Reissner E (1947), On bending of elastic plates, *Quarterly of Applied Mathematics* **5**, 55–68.

[11] Knowles J and Wang N (1960), On the bending of an elastic plate containing a crack, *Journal of Mathematics and Physics* **39**, 223–236.

[12] Wang N (1968), Effects of plate thickness on the bending of an elastic plate containing a crack, *Journal of Mathematics and Physics* **47**, 371–390.

[13] Hartranft RJ and Sih GC (1968), Effect of plate thickness on the bending stress distribution around through cracks, *Journal of Mathematics and Physics* **47**, 276–291.

[14] Wang N (1970), Twisting of an elastic plate containing a crack, *International Journal of Fracture Mechanics* **6**, 367–378.

[15] Tamate O (1975), A theory of dislocations in the plate under flexure with application to crack problems, Tech. rep., Tohoku University, technology Report 40(1):67–88.

[16] Delale F and Erdogan F (1981), Line-spring model for surface cracks in a Reissner plate, *International Journal of Engineering Science* **19**, 1331–1340.

[17] Irwin G (1957), Analysis of stresses and strains near the end of a crack traversing a plate, *Journal of Applied Mechanics* **24**, 361–364.

[18] Rice J (1968), A path independent integral and the approximate analysis of strain concentration by notches and cracks, *Journal of Applied Mechanics* **35**, 379–386.

[19] Viz M, Potyondy D, Zehnder A, Rankin C, and Riks E (1995), Computation of membrane and bending stress intensity factors for thin, cracked plates, *International Journal of Fracture* **72**, 21–38.

[20] Lemaitre J, Turbat A, and Loubet R (1977), Fracture mechanics analysis of pressurized cracked shallow shells, *Engineering Fracture Mechanics* **9**, 443–460.

[21] Young M and Sun C (1993), On the strain energy release rate for a cracked plate subjected to out-of-plane bending moment, *International Journal of Fracture* **60**, 227–247.

[22] Young M and Sun C (1993), Cracked plates subjected to out-of-plane tearing loads, *International Journal of Fracture* **60**, 1–18.

[23] Simmonds J and Duva J (1981), Thickness effects are minor in the energy release rate integral for bent plates containing elliptic holes or cracks, *Journal of Applied Mechanics* **48**, 320–326.

[24] Joseph PF and Erdogan F (1989), Surface crack problems in plates, *International Journal of Fracture* **41**, 105–131.

[25] Murakami Y (1987), *Stress Intensity Factors Handbook*, vol. 2, Pergamon Press, Elmsford, New York.

[26] Zehnder A and Hui CY (1994), Stress intensity factors for plate bending and shearing problems, *Journal of Applied Mechanics* **61**, 719–722.

[27] Hasebe N, Matsuura S, and Kondo N (1984), Stress analysis of a strip with a step and a crack, *Engineering Fracture Mechanics* **20**, 447–462.

[28] Joseph PF and Erdogan F (1991), Bending of a thin reissner plate with a through crack, *Journal of Applied Mechanics* **58**, 842–846.

[29] Murthy M, Raju K, and Viswanath S (1981), On the bending stress distribution at the tip of a stationary crack from Reissner's theory, *International Journal of Fracture* **17**, 537–552.

[30] Boduroglu H and Erdogan F (1983), Internal and edge cracks in a plate of finite width under bending, *Journal of Applied Mechanics* **50**, 621–629.

[31] Sih GC (1977), *Mechanics of Fracture 3: Plates and Shells with Cracks*, Noordhoff International, Leyden.

[32] Alwar RS and Ramachandran KNN (1983), Three-dimensional finite element analysis of cracked thick plates in bending, *International Journal for Numerical Methods in Engineering* **19**, 293–303.

[33] Barsoum RS (1976), A degenerate solid element for linear fracture analysis of plate bending and general shells, *International Journal for Numerical Methods in Engineering* **10**, 551–564.

[34] Rhee HC and Atluri SN (1982), Hybrid stress finite element analysis of plate bending and general shells, *International Journal for Numerical Methods in Engineering* **18**, 259–271.

[35] Zucchini A, Hui CY, and Zehnder AT (2000), Crack tip stress fields for thin plates in bending, shear and twisting: A comparison of plate theory and three dimensional elasticity theory, *International Journal of Fracture* **104**, 387–407.

[36] Mullinix BR and Smith CW (1974), Distribution of local stresses across the thickness of cracked plates, *International Journal of Fracture* **10**, 337–352.

[37] Hui CY, Zehnder AT, and Potdar YK (1998), Williams meets von-Karman: Mode coupling and non-linearity in the fracture of thin plates, *International Journal of Fracture* **93**, 409–429.

[38] von Kármán T (1910), Festigkeitsprobleme in maschinenbau, *Encyklopadia der Mathematischen Wissenschaften, IV* **Chap. 27**, 311–385.

[39] Johnson W (1986), Stress analysis of the cracked lap shear specimen: An ASTM round robin, Tech. rep., National Aeronautics and Space Administration, NASA TM 89006.

[40] Frisch J (1961), Fracture of flat and curved aluminum sheets with stiffeners parallel to the crack, *Journal of Basic Engineering* **83**, 32–38.

[41] Folias E (1970), On the theory of fracture of curved sheets, *Engineering Fracture Mechanics* **2**, 151–164.

[42] Folias E (1965), A finite line crack in a pressurized spherical shell, *International Journal of Fracture Mechanics* **1**, 20–46.

[43] Folias E (1965), An axial crack in a pressurized cylindrical shell, *International Journal of Fracture Mechanics* **1**, 104–113.

[44] Folias E (1967), A circumferential crack in a pressurized cylindrical shell, *International Journal of Fracture Mechanics* **3**, 1–11.

[45] Folias E (1969), On the effect of initial curvature on cracked flat sheets, *International Journal of Fracture Mechanics* **5**, 327–346.

[46] Copley L and Sanders J (1969), A longitudinal crack in a cylindrical shell under internal pressure, *International Journal of Fracture Mechanics* **5**, 117–131.

[47] Duncan M and Sanders J (1969), The effect of a circumferential stiffener on the stress in a pressurized cylindrical shell with a longitudinal crack, *International Journal of Fracture Mechanics* **5**, 133–155.

[48] Yashi OS and Erdogan F (1983), A cylindrical shell with an arbitrarily oriented crack, *International Journal of Solids and Structures* **19**, 955–972.

[49] Alabi JA and Sanders JL (1985), Circumferential crack at the end of a fixed pipe, *Engineering Fracture Mechanics* **22**, 609–616.

[50] Alabi JA (1987), Circumferential crack at the fixed end of a cylinder in flexure, *Journal of Applied Mechanics* **54**, 861–865.

[51] Erdogan F and Ratwani M (1972), A circumferential crack in a cylindrical shell under torsion, *International Journal of Fracture* **8**, 87–95.

[52] Xie YJ (2000), An analytical method on circumferential periodic cracked pipes and shells, *International Journal of Solids and Structures* **37**, 5189–5201.

[53] Simmonds JG, Bradley MR, and Nicholson JW (1978), Stress-intensity factors for arbitrarily oriented cracks in shallow shells, *Journal of Applied Mechanics* **45**, 135–141.

[54] Huang NC, Li YC, and Russell SG (1997), Fracture mechanics of plates and shells applied to fail-safe analysis of fuselage part I: Theory, *Theoretical and Applied Fracture Mechanics* **27**, 221–236.

[55] Erdogan F and Kibler J (1969), Cylindrical and spherical shells with cracks, *International Journal of Fracture Mechanics* **5**, 229–237.

[56] Erdogan F and Ratwani M (1972), Fracture of cylindrical and spherical shells containing a crack, *Nuclear Engineering and Design* **20**, 265–286.

[57] Smith D and Smith C (1970), A photoelastic evaluation of the influence of closure and other effects upon the local bending stresses in cracked plates, *International Journal of Fracture Mechanics* **6**, 305–318.

[58] Jones D and Swedlow J (1975), The influence of crack closure and elasto-plastic flow on the bending of a cracked plate, *International Journal of Fracture* **11**, 897–914.

[59] Young M and Sun C (1992), Influence of crack closure on the stress intensity factor in bending plates—A classical plate solution, *International Journal of Fracture* **55**, 81–93.

[60] Heming FS (1980), Sixth order analysis of crack closure in bending of an elastic plate, *International Journal of Fracture* **16**, 289–304.

[61] Alwar RS and Ramachandran KNN, Influence of crack closure on the stress intensity factor for plates subjected to bending - a 3-D finite element analysis, *Engineering Fracture Mechanics* **17**, 323–333.

[62] M V V Murthy aVKM S Viswanath and Rao KP (1988), A two-dimensional model for crack closure effect in plates under bending, *Engineering Fracture Mechanics* **29**, 77–117.

[63] Delale F and Erdogan F (1979), The effect of transverse shear in a cracked plate under skew-symmetric loading, *Journal of Applied Mechanics* **46**, 618–624.

[64] Slepyan LI, Dempsey JP, and Shekhtman II (1995), Asymptotic solutions for crack closure in an elastic plate under combined extension and bending, *Journal of the Mechanics and Physics of Solids* **43**, 1727–1749.

[65] Dempsey JP, Shektman II, and Slepyan LI (1998), Closure of a through crack in a plate under bending, *International Journal of Solids and Structures* **35**, 4077–4089.

[66] Parks D (1974), A stiffness derivative finite element technique for determination of crack tip stress intensity factors, *International Journal of Fracture* **10**, 487–502.

[67] Ansell H (1988), *Bulging of Cracked Pressurized Aircraft Structures, Report No.* LIU–TEK–LIC 1988:11, Ph.D., Linköping University.

[68] Rybicki E and Kanninen M (1977), A finite element calculation of stress intensity factors by a modified crack closure integral, *Engineering Fracture Mechanics* **9**, 931–938.

[69] Viz MJ (1996), *Fatigue fracture of 2024-T3 aluminum plates under combined in-plane symmetric and out-of-plane antisymmetric mixed-mode deformations*, Ph.D., Cornell University.

[70] Frangi A (1997), Regularized BE formulations for the analysis of fracture in thin plates, *International Journal of Fracture* **84**, 351–366.

[71] Frangi A and Guiggiani M (1999), Boundary element analysis of Kirchhoff plates with direct evalulation of hypersingular integrals, *International Journal for Numerical Methods in Engineering* **46**, 1845–1863.

[72] Su RKL and Sun HY (2002), Numerical solution of cracked thin plates subjected to bending, twisting and shear loads, *International Journal of Fracture* **117**, 323–335.

[73] Wilson WK and Thompson DG (1971), On the finite element method for calculating stress intensity factors for cracked plates in bending, *Engineering Fracture Mechanics* **3**, 97–102.

[74] Chen WH and Chen PY (1984), A hybrid-displacement finite element model for the bending analysis of thin cracked plates, *International Journal of Fracture* **24**, 83–106.

[75] Chen WH, Yang KC, and Chang CS (1984), A finite element alternating approach for the bending analysis of thin cracked plates, *International Journal of Fracture* **24**, 83–106.

[76] Ahmad J and Loo FTC (1979), Solution of plate bending problems in fracture mechanics using a specialized finite element technique, *Engineering Fracture Mechanics* **11**, 661–673.

[77] Chen W and Shen C (1993), A finite element alternating approach to the bending of thin plates containing mixed mode cracks, *International Journal of Solids and Structures* **30**, 2261–2276.

[78] Dolbow J, Moes N, and Belytschko T (2000), Modeling fracture in Mindlin-Reissner plates with the extended finite element method, *International Journal of Solids and Structures* **37**, 7161–7183.

[79] Yau J, Wang S, and Corten H (1980), A mixed-mode crack analysis of isotropic solids using conservation laws of elasticity, *Journal of Applied Mechanics* **47**, 335–341.

[80] Dirgantara T and Aliabadi MH (2001), Dual boundary element formulation for fracture mechanics analysis of shear deformable shells, *International Journal of Solids and Structures* **38**, 7769–7800.

[81] Dirgantara T and Aliabadi MH (2002), Stress intensity factors for cracks in thin plates, *Engineering Fracture Mechanics* **69**, 1465–1486.

[82] Dirgantara T and Aliabadi MH (2002), Numerical simulation of fatigue crack growth in pressurized shells, *International Journal of Fatigue* **24**, 725–738.

[83] Wen PH, Aliabadi MH, and Young A (2003), Fracture mechanics analysis of curved stiffened panels using bem, *International Journal of Solids and Structures* **40**, 219–236.

[84] Riks E and denReijer P (1987), Finite element analysis of cracks in a thin walled cylinder under internal pressure, Tech. rep., National Aerospace Laboratory, Amsterdam, Netherlands, report No. NLR–TR–87021–U, NTIS No. PB88–241021.

[85] Riks E (1987), Bulging cracks in pressurized fuselages: A numerical study, Tech. rep., National Aerospace Laboratory, Amsterdam, Netherlands, report No. NLR–MP–87058–U, NTIS No. PB89–153340.

[86] Chen D and Schijve J (1991), Bulging of fatigue cracks in a pressurized aircraft fuselage, in Kobayashi A (ed.) *Aeronautical fatigue: Key to safety and structural integrity; Proceedings of the 16th* ICAF *Symposium, Tokyo, Japan, May 22-24, 1991*, International Committee on Aeronautical Fatigue, EMAS Publishing.

[87] Chen CS, Wawrzynek P, and Ingraffea AR (2002), Prediction of residual strength and curvilinear crack growth in aircraft fuselages, *AIAA Journal* **40**, 1644–1652.

[88] Chen CS, Wawrzynek P, and Ingraffea AR (1999), Residual strength prediction in kc-135 fuselages and curvilinear crack growth analysis in narrow body fuselages, in *Third Joint FAA-DoD-NASA Conference on Aging Aircraft*.

[89] Huang NC, Li YC, and Russell SG (1997), Fracture mechanics of plates and shells applied to fail-safe analysis of fuselage part II: Computational results, *Theoretical and Applied Fracture Mechanics* **27**, 237–253.

[90] Erdogan F, Tuncel O, and Paris P (1962), An experimental investigation of the crack tip stress intensity factors in plates under cylindrical bending, *Journal of Basic Engineering* **84**, 542–546.

[91] Wynn R and Smith C (1969), An experimental investigation of fracture criteria for combined extension and bending, *Journal of Basic Engineering* **91**, 841–849.

[92] Saint-John C and Street K (1974), B-Al composite failure under combined torsion and tension loading, *Journal of Composite Materials* **8**, 266–274.

[93] Ewing PD and Williams JG (1974), Fracture of spherical-shells under pressure and circular tubes with angled cracks in torsion, *International Journal of Fracture* **10**, 537–544.

[94] Bastun VN (1994), Fracture of thin-walled bodies with crack under biaxial loading, *Engineering Fracture Mechanics* **48**, 703–709.

[95] Viz MJ, Zehnder AT, and Bamford JD (1995), Fatigue fracture of thin plates under tensile and transverse shearing stresses, in Reuter W (ed.) *Fracture Mechanics, 26th Volume*, vol. ASTM STP 1256, American Society for Testing and Materials, 631–651.

[96] Zehnder AT, Viz MJ, and Potdar YK (2000), Fatigue fracture in plates under tension and out-of-plane shear, *Fatigue and Fracture of Engineering Materials and Structures* **23**, 403–415.

[97] Tschegg E, Ritchie R, and McClintock F (1983), On the influence of rubbing fracture surfaces on fatigue crack propagation in mode III, *International Journal of Fatigue* **5**, 29–35.

[98] Tschegg E and Suresh S (1988), Mode III fracture of 4340 steel: Effects of tempering temperature and fracture surface interference, *Metallurgical Transactions A* **19A**, 3035–3044.

[99] Gross T (1985), Frictional effects in mode III fatigue crack propagation, *Scripta Metallurgica* **19**, 1185–1188.

[100] Narasimhan R and Rosakis AJ (1988), A finite element analysis of small scale yielding near a stationary crack under plane stress, *Journal of the Mechanics and Physics of Solids* **36**, 77–117.

[101] Hudson C (1969), Effect of stress ratio on fatigue-crack growth in 7075–T6 and 2024–T3 aluminum-alloy specimens, Tech. rep., National Aeronautics and Space Administration, NASA TN D-5390.

List of Figures

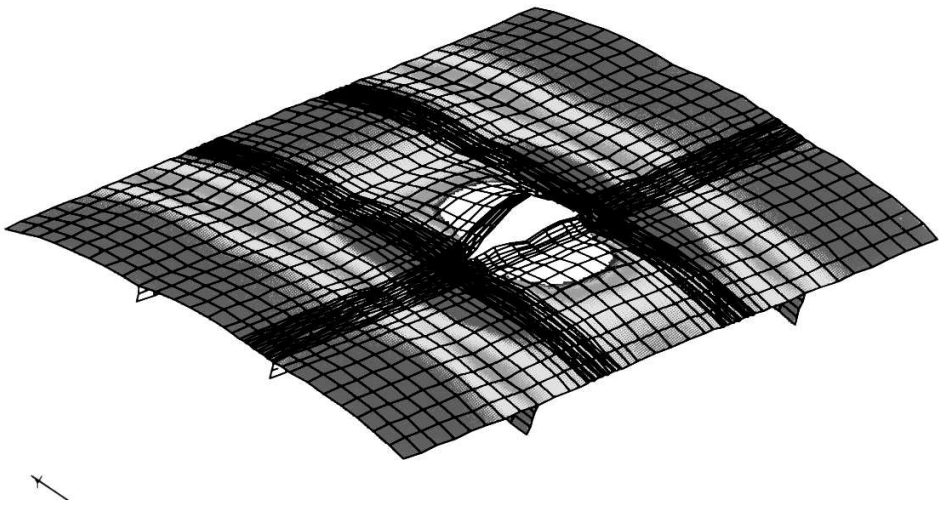

Figure 1: FEM simulation of a crack along a lap joint in a pressurized fuselage. Fuselage bulges out on one side of the lap joint, resulting in crack tip out-of-plane shearing stresses. Courtesy of Dr. V. Britt, formerly NASA Langley Aircraft Structures Branch.

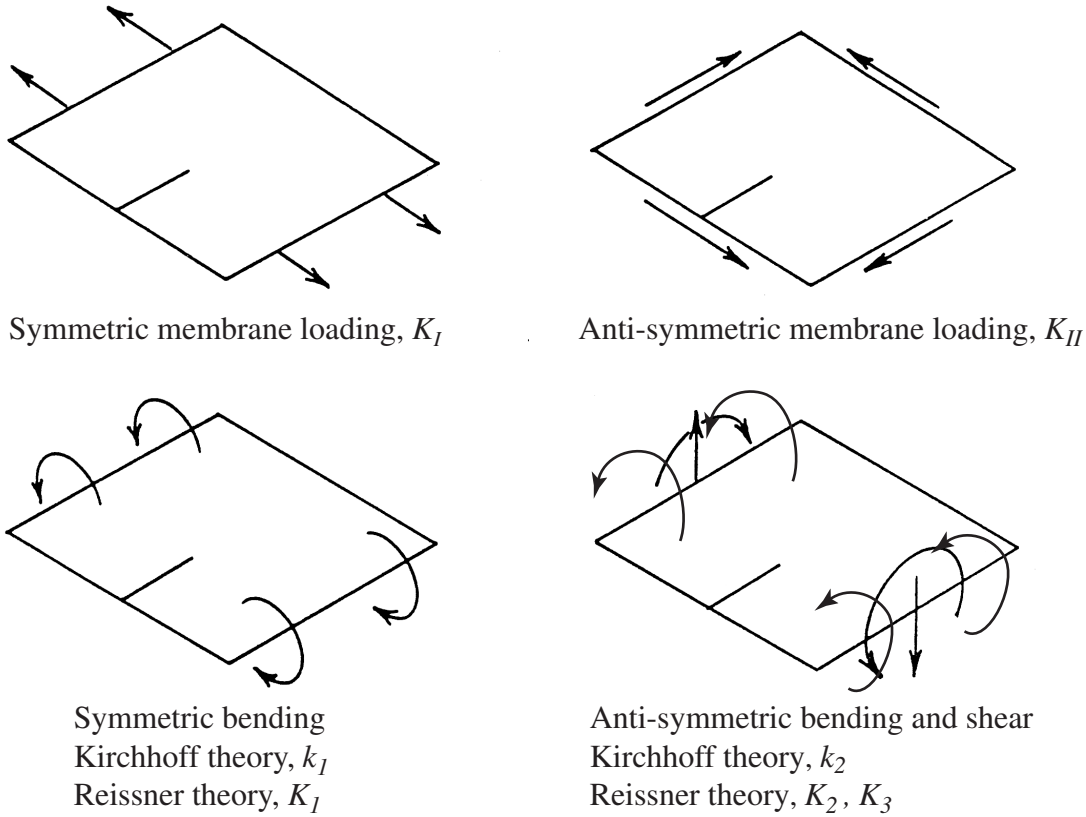

Figure 2: Membrane, bending and transverse shear fracture modes for a plate with a straight through crack. Stress intensity factors corresponding to each mode are shown.

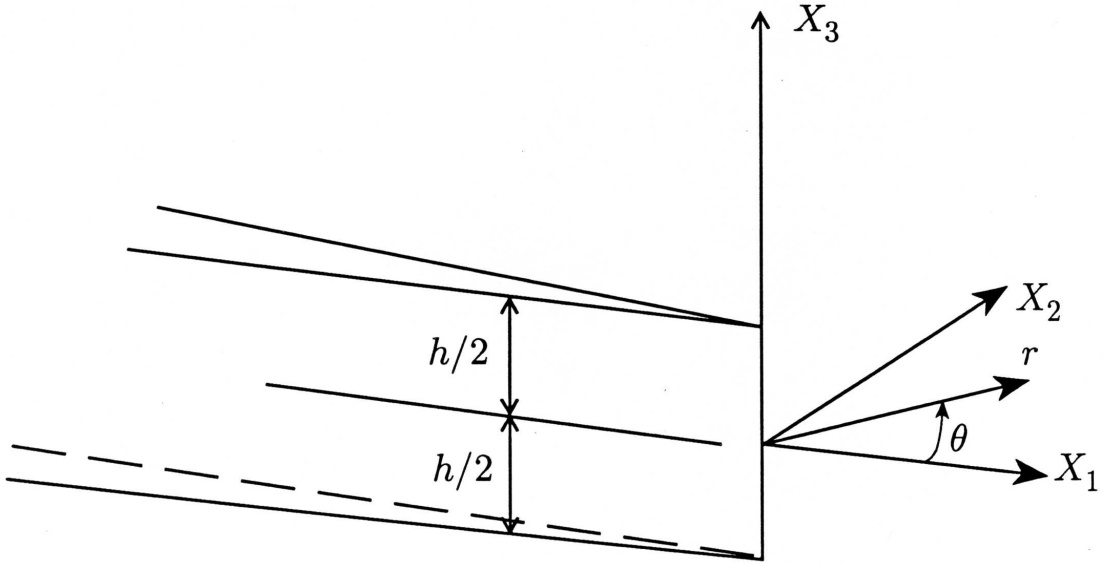

Figure 3: Coordinate system at the tip of a crack in a plate or shell.

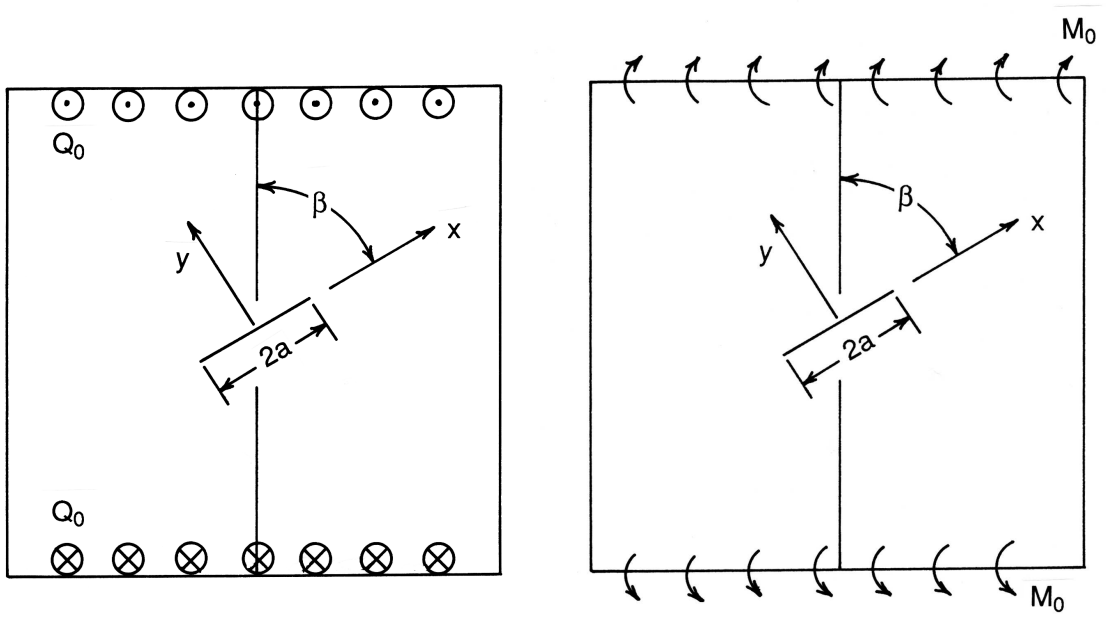

(a) (b)

Figure 4: Finite crack at angle β to the loading in an infinite plate. (a) Uniform far field transverse shearing. Moments needed for equilibrium are omitted for clarity. (b) Uniform far-field bending moment.

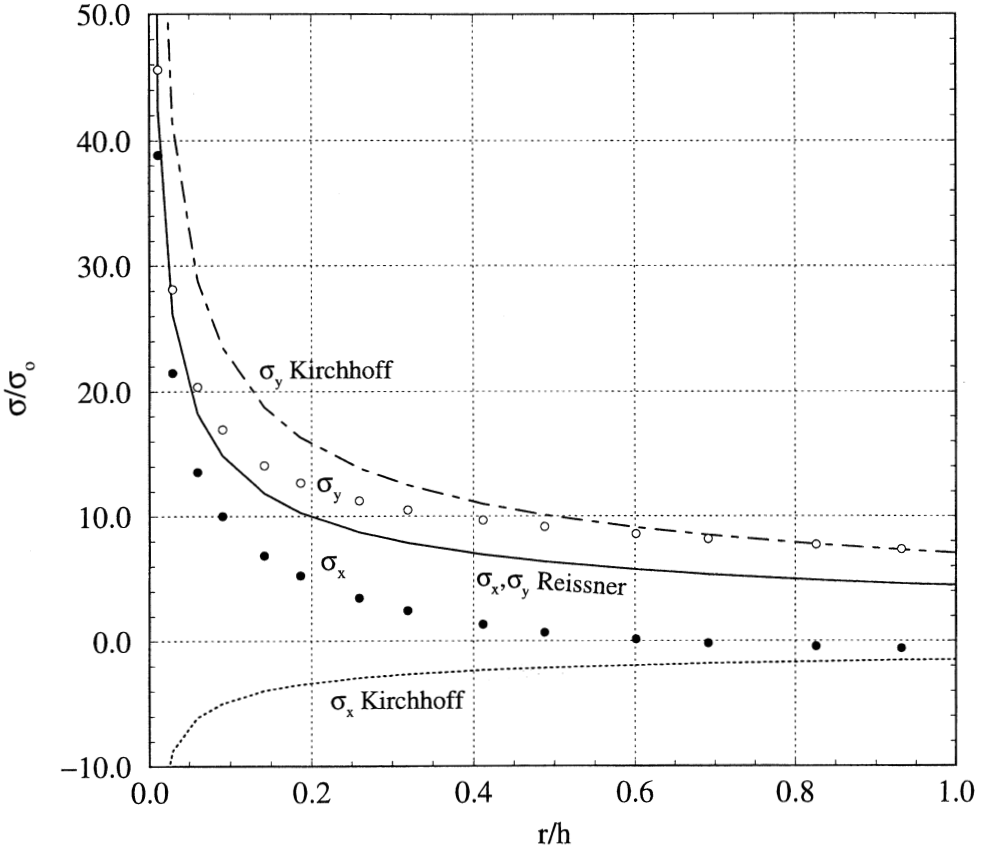

Figure 5: Thin, cracked plate, $(h/a = 0.02)$, where h is the plate thickness and a is the crack half-length, under symmetric bending. Normal stresses at the surface vs. radial distance from the crack as predicted by 3-D analysis, Reissner and Kirchhoff theories. σ_0 is the far field surface tensile stress.

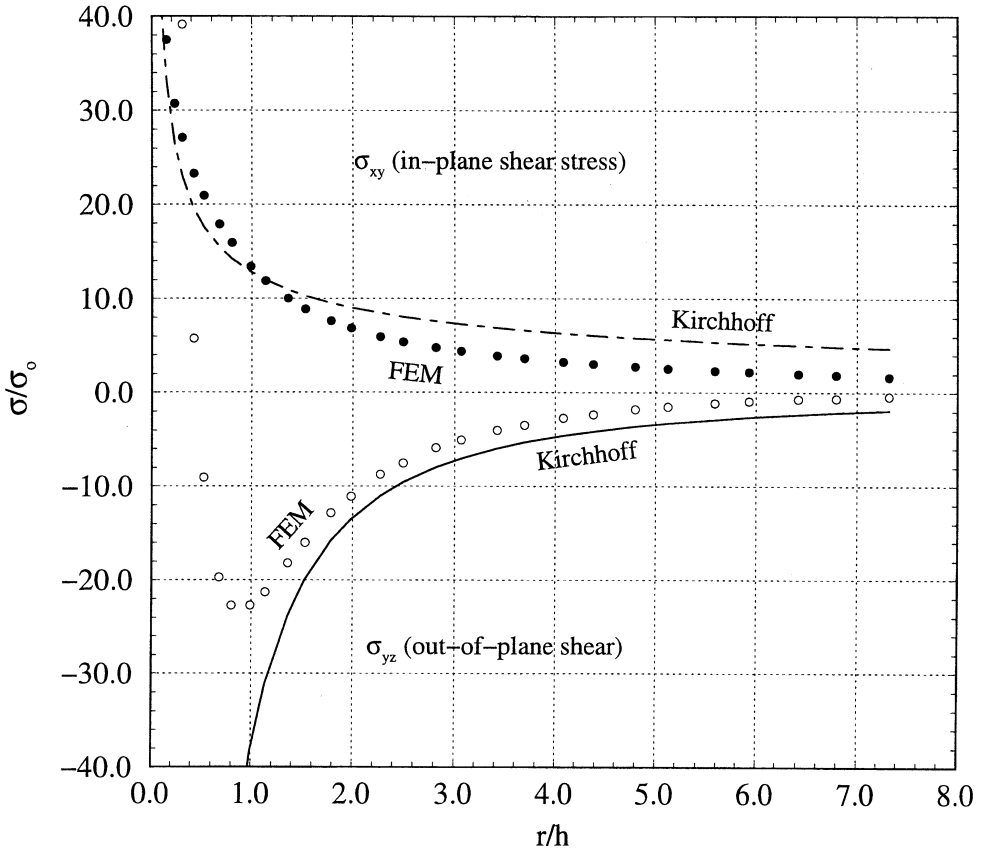

Figure 6: Thin, cracked plate under uniform shear. Mid-plane shear stresses, σ_{32} (σ_{yz} in figure) and σ_{12} (σ_{xy} in figure) versus distance from the crack tip, along $x_2 = 0$, as predicted by Kirchhoff theory and 3-D FEM analysis. σ_0 is the far-field mid-plane shear stress.

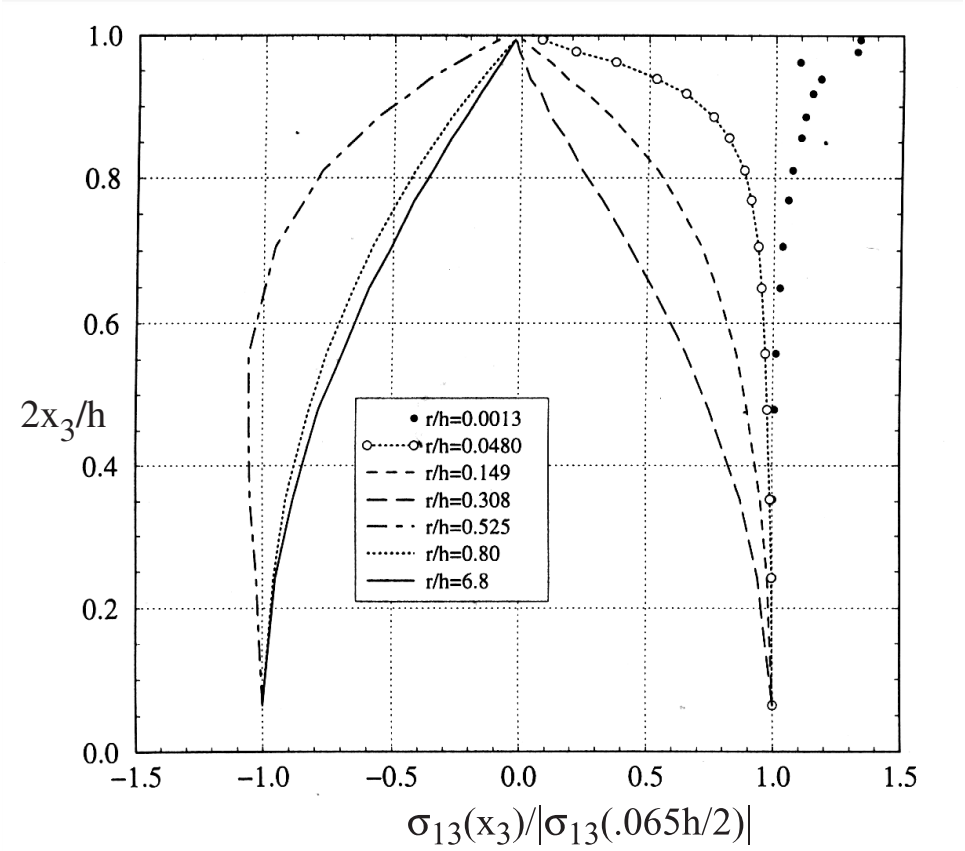

Figure 7: Thin, cracked plate under uniform shear ($h/a = 0.024$, $\nu = .3$). Distributions of the shear stress σ_{13} through the thickness from 3D finite element analysis at different radial distances from the crack tip.

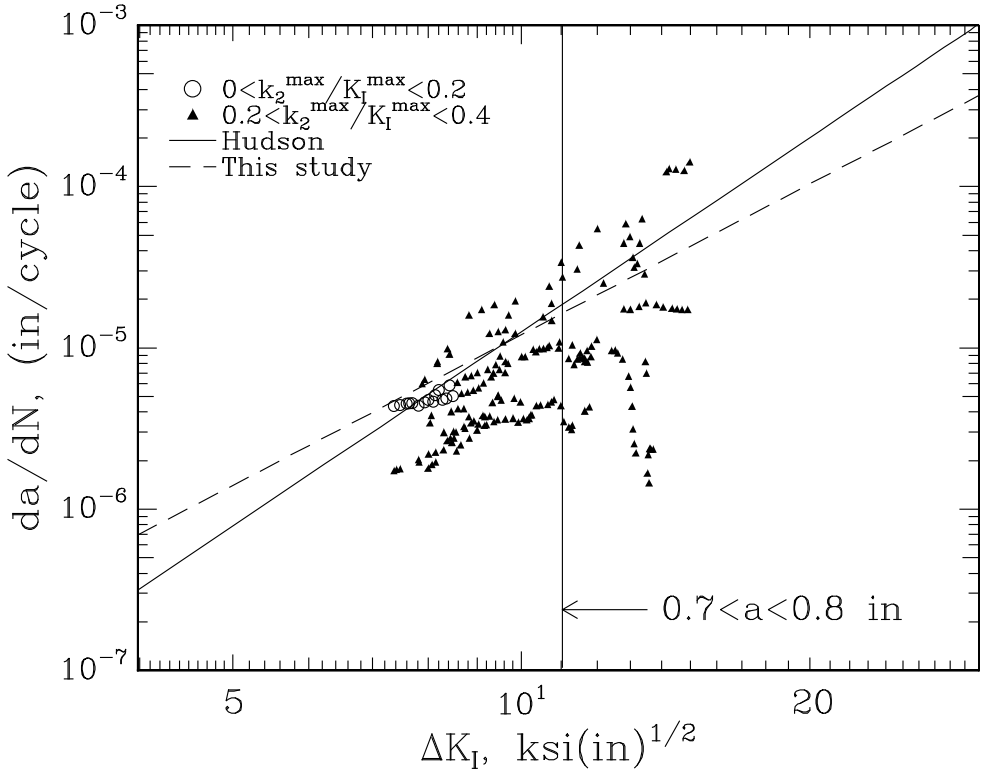

Figure 8: Mixed-mode fatigue crack growth rate results. The solid (Hudson [101]) and dashed (Viz [69, 96]) lines represent the crack growth rate for pure Mode-I loading. The vertical line indicates the range of crack lengths present in this data when $\Delta K_I = 11 ksi\sqrt{in}$. $R = 0.7$. Data are plotted only for relatively low values of k_2.

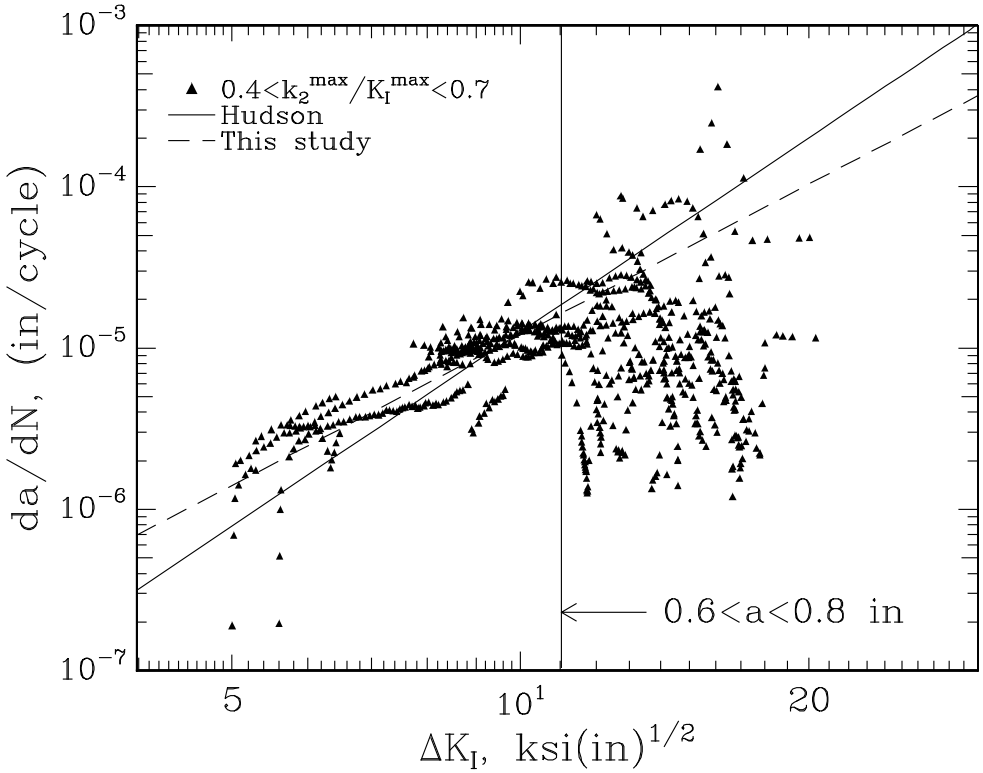

Figure 9: Same as Figure 7, for medium range of values of k_2.

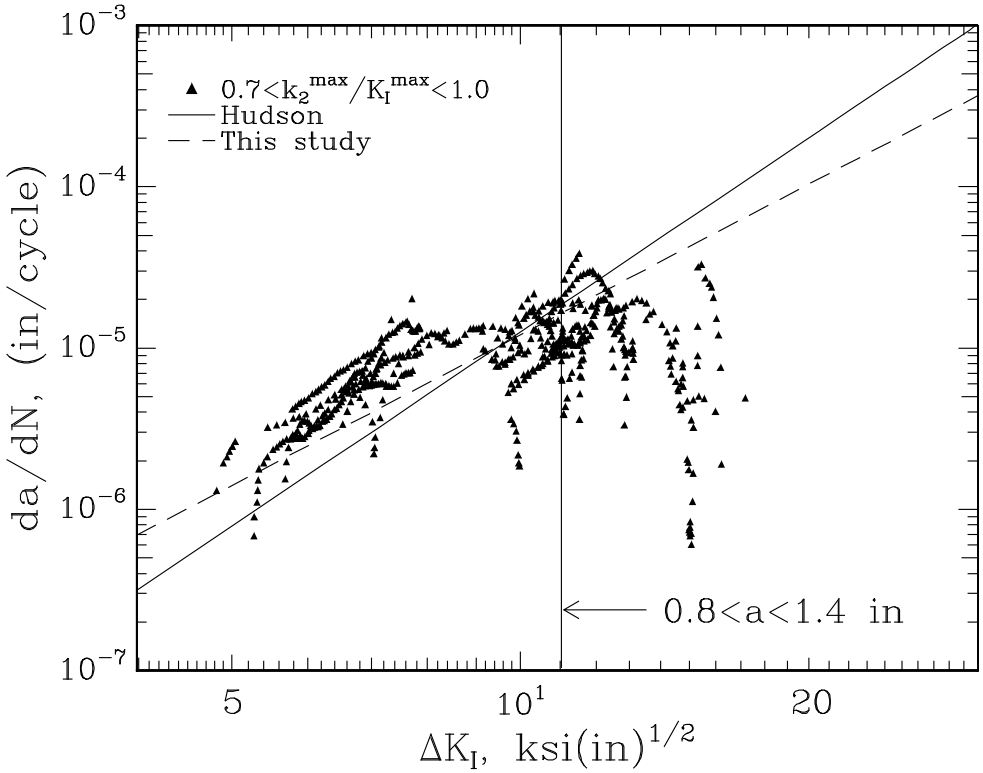

Figure 10: Same as Figure 7, for relatively large values of k_2.

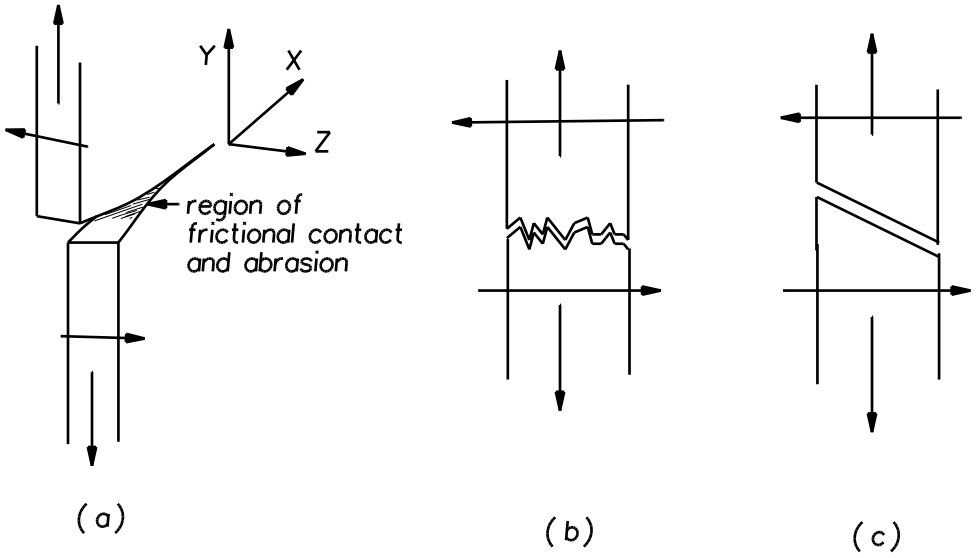

Figure 11: Fracture in plates and shells under tension and out-of-plane shearing. (a) The surfaces behind the crack can be in contact, resulting in frictional and normal tractions that shield the crack tip from the full measure of stress variation, reducing crack growth rate. (b) The loss of indexing of mating fracture surfaces due to out-of-plane displacement results in increased normal traction and shear traction due to asperities trying to slide through each other. (c) Cracks often grow on a slant in the orientation shown, resulting in greatly increased out-of-plane shear and normal shielding tractions.

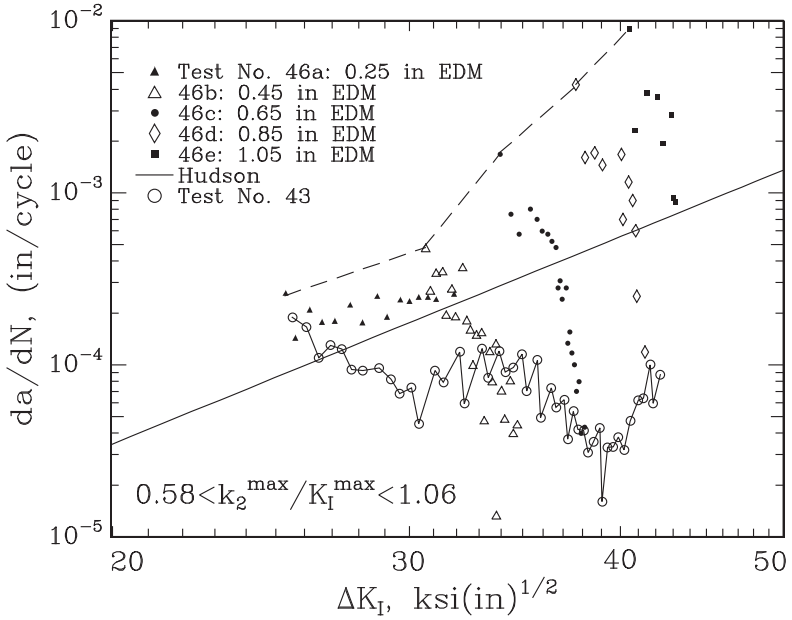

Figure 12: Mixed-mode fatigue crack growth rate in the absence of crack contact (dashed line) and with contact (solid line connecting points.) $R = 0.1$.